Altered Structural Brain Connectivity in Healthy Carriers of the Autism Risk Gene, *CNTNAP2*

Emily L. Dennis,[1] Neda Jahanshad,[1] Jeffrey D. Rudie,[2] Jesse A. Brown,[3] Kori Johnson,[4,5]
Katie L. McMahon,[4] Greig I. de Zubicaray,[6] Grant Montgomery,[5] Nicholas G. Martin,[5] Margaret J. Wright,[5,6]
Susan Y. Bookheimer,[3] Mirella Dapretto,[2] Arthur W. Toga,[1] and Paul M. Thompson[1]

Abstract

Recently, carriers of a common variant in the autism risk gene, *CNTNAP2*, were found to have altered functional brain connectivity using functional MRI. Here, we scanned 328 young adults with high-field (4-Tesla) diffusion imaging, to test the hypothesis that carriers of this gene variant would have altered structural brain connectivity. All participants (209 women, 119 men, age: 23.4 ± 2.17 SD years) were scanned with 105-gradient high-angular-resolution diffusion imaging (HARDI) at 4 Tesla. After performing a whole-brain fiber tractography using the full angular resolution of the diffusion scans, 70 cortical surface-based regions of interest were created from each individual's co-registered anatomical data to compute graph metrics for all pairs of cortical regions. In graph theory analyses, subjects homozygous for the risk allele (CC) had lower characteristic path length, greater small-worldness and global efficiency in whole-brain analyses, and lower eccentricity (maximum path length) in 60 of the 70 nodes in regional analyses. These results were not reducible to differences in more commonly studied traits such as fiber density or fractional anisotropy. This is the first study that links graph theory metrics of brain structural connectivity to a common genetic variant linked with autism and will help us understand the neurobiology of the circuits implicated in the risk for autism.

Key words: autism; *CNTNAP2*; graph theory; HARDI; structural connectivity; twins

Introduction

MANY NEUROPSYCHIATRIC DISORDERS are thought to involve disrupted brain connectivity, but very little is known about what causes brain connectivity to vary in human populations. Total brain volume (Posthuma et al., 2000), cortical thickness (Schmitt et al., 2008; Thompson et al., 2001), and measures of white matter integrity derived from diffusion tensor imaging (DTI) (Chiang et al., 2009, 2011a; Pfefferbaum et al., 2001) are all under moderately strong genetic control. By analyzing very large cohorts (on the order of 20,000 subjects) with MRI and genome-wide scans (Stein et al., 2012), we recently discovered commonly carried genetic variants that are associated with differences in brain structure. Since these studies searched the genome for effects of up to a million single nucleotide polymor-

phisms (SNPs), very large samples were needed to reduce the risk of false-positive associations. An alternative approach is to study the candidate genes already associated with disease risk. For instance, young adults who carry the Alzheimer's risk allele *CLU*-C have lower white matter integrity in DTI scans of the brain, as measured by fractional anisotropy (FA) (Braskie et al., 2011). In addition, common variants in the growth factor genes, *BDNF* and *NTRK1*, are also associated with altered white matter integrity, making it possible to predict a small proportion of individual differences in brain integrity by genotyping multiple common variants (Kohannim et al., 2011). These early DTI genetics studies have generally mapped brain integrity using maps of FA, either broadly across the brain (Braskie et al., 2011), or in specific brain regions (Chiang et al., 2009; McIntosh et al., 2008; Winterer et al., 2008). Methods that assess brain

[1]Laboratory of Neuro Imaging, UCLA School of Medicine, Los Angeles, California.
[2]Ahmanson Lovelace Brain Mapping Center, UCLA, Los Angeles, California.
[3]Center for Cognitive Neuroscience, UCLA, Los Angeles, California.
[4]Center for Advanced Imaging, University of Queensland, Brisbane, Australia.
[5]Queensland Institute of Medical Research, Brisbane, Australia.
[6]School of Psychology, University of Queensland, Brisbane, Australia.

connectivity may be useful in gauging how these variants affect white matter organization overall. Even so, no studies have yet linked the graph metrics of structural brain connectivity to any specific genetic variants. The power to detect gene effects is limited in small samples, so we scanned a fairly large cohort of twins (118 identical twins, 183 fraternal twins, and 27 nontwin siblings) with high angular resolution diffusion imaging (HARDI), at a relatively high magnetic field (4 Tesla).

The recently discovered autism risk gene, *CNTNAP2*, encodes CASPR2, or contactin-associated protein-like 2, a member of the neurexin superfamily of transmembrane proteins. CASPR2 is involved in clustering voltage-gated potassium channels (K_v1.1) at the nodes of Ranvier (Strauss et al., 2006; Vernes et al., 2008). CASPR2 has a suggested developmental role as a cell adhesion molecule responsible for neuroblast migration and laminar organization (Arking et al., 2008; Bakkaloglu et al., 2008; Vernes et al., 2008). In a study of an Amish family, a deletion mutation in *CNTNAP2* was linked with a disorder with many hallmarks of autism, involving seizures, language difficulties, and impaired social abilities (Strauss et al., 2006). Subsequent research in both autistic and language-impaired (but nonautistic) populations has discovered further support that *CNTNAP2* is associated with autism (Alarcón et al., 2008; Arking et al., 2008; Bakkaloglu et al., 2008) and language ability (Alarcón et al., 2008; Vernes et al., 2008). A recent study characterizing *CNTNAP2* knockout mice found behavioral deficits characteristic of autism—namely, seizures—as well as neuronal migration abnormalities, reduced interneuron density, and abnormal neuronal network activity (Peñagarikano et al., 2011). *CNTNAP2* expression is highest in the frontal and temporal lobes (Abrahams et al., 2007; Arking et al., 2008; Bakkaloglu et al., 2008; Vernes et al., 2008), areas responsible for language abilities, particularly in the left hemisphere (Baynes et al., 1998), supporting the link between *CNTNAP2* and language function. Stein et al. (2011) found that a *CNTNAP2* SNP (rs2710102) was associated with increased risk for selective mutism, an anxiety disorder in which a child is unable or unwilling to speak in certain situations, despite having normal language abilities in other situations. This disorder is similar, in some respects, to autism; they both involve characteristic deficits in language and social interactions.

In a recent analysis of *functional* brain connectivity using functional MRI, Scott-Van Zeeland et al. (2010) compared risk and nonrisk allele carriers of *CNTNAP2* (rs2710102) in a cohort consisting of both autistic and typically developing children. Children with the genetic risk allele did not show the same left-lateralized pattern of medial prefrontal cortex connectivity as noncarriers. This association was consistent with previous research linking *CNTNAP2* to language ability. Scott-Van Zeeland et al. also found stronger long-range anterior-posterior connections in the nonrisk subjects and stronger short-range frontal lobe connectivity in the at-risk subjects. Since short-range connections are typically pruned and long-range ones are strengthened over the course of development (Dosenbach et al., 2010; Huttenlocher, 1990), this may be evidence of delayed development in those at risk.

The graph theory can quantify brain connectivity at the network level. This branch of mathematics—for describing and analyzing graphs—examines brain networks as collections of nodes (i.e., specific brain regions) and edges (connections between those regions) (Sporns et al., 2004). The complex web of brain structural or functional connectivity may be quantified using a number of key parameters that summarize network characteristics. Path length, for example, is a measure of the distance (i.e., number of edges) between one brain region and another (Rubinov and Sporns, 2010). A network with a shorter average path length is considered more efficient in terms of information transfer (Bullmore and Sporns, 2009). We recently found these metrics to be heritable in this same sample (Dennis et al., 2011).

Here, we set out to investigate how variations in a *CNTNAP2* SNP (rs2710102) might relate to graph theoretical measures from diffusion-weighted MRI. Further impetus for this work came from a recent report that found an association between a different *CNTNAP2* SNP (rs7794745) and FA (Tan et al., 2010). Tan et al. (2010) found lower FA in individuals homozygous for the risk allele in a number of regions implicated in autism, including the cerebellum, fusiform gyrus, occipital, and frontal cortices. Given this previous success in linking a different *CNTNAP2* SNP with structural connectivity, we decided that this might be a promising method for understanding the results of Scott-Van Zeeland et al., who found an association between our *CNTNAP2* SNP (rs2710102) and alterations in functional connectivity. Functional and structural connectivity are closely related, with functional connectivity existing between areas that are structurally connected; yet functional connections may exist where no structural connections exist (Honey et al., 2009). Results from these different modalities may assess different types of connectivity, but they are complementary and together generate a more complete picture of brain networks. In some cases but not others, differences in functional synchronization may be explained by detectable differences in structural connections. Additionally, findings from different modalities may discover the general principles of neural organization from multiple very different modalities, such as network hubs, small-world properties, as well as metrics of efficiency and resilience to disruption. Previous research associating *CNTNAP2* with cognitive or behavioral traits focused on autistic populations or people with known language difficulties. To test whether this very common genetic variant leads to detectable brain differences outside of populations with language or developmental disorders, we focused on healthy adults with normal variations in language ability. Since Scott-Van Zeeland et al. (2010) were able to find and replicate *CNTNAP2*'s association with brain connectivity in a population of both autistic and typically developing children, we hypothesized that we might be able to detect differences in the structural networks of healthy normal carriers of the *CNTNAP2* risk allele (rs2710102). In this study, we assessed both global and hemisphere-specific brain network properties. We recently reported on genetically influenced left-right asymmetries in white matter tracts (Jahanshad et al., 2010). Given those asymmetries, we expected that the relationship between *CNTNAP2* and network measures might differ by hemisphere, as *CNTNAP2* is linked with language ability (Alarcón et al., 2008; Vernes et al., 2008)—a generally left-lateralized function (Baynes et al., 1998). As such, we tested for the effects on each hemisphere independently.

Materials and Methods

Participants

Participants were recruited as part of a 5-year research project examining healthy young adult Australian twins using structural MRI and DTI with a projected sample size of ~1150 at completion (de Zubicaray et al., 2008). Our analysis included 328 right-handed subjects (209 women/119 men, average age = 23.4, SD = 2.17). This population included 118 monozygotic (MZ) twins, 183 dizygotic (DZ) twins, and 27 nontwin siblings, from 189 families. The population was racially homogenous: 100% of subjects were Caucasian. In studies of genetic variations, a genetically homogenous population is preferable to avoid incorrectly ascribing effects to alleles that have different frequencies in different racial/ethnic groups. The subjects were screened to exclude those with a history of significant head injury, neurological or psychiatric illness, substance abuse or dependence, or who had a first-degree relative with a psychiatric disorder. All the participants were right handed, as assessed by 12 items on the Annett's Handedness Questionnaire (Annett, 1970). The study participants gave informed consent; the institutional ethics committees at the Queensland Institute of Medical Research, the University of Queensland, the Wesley Hospital, and at UCLA approved the study.

Establishing zygosity and genotyping

Zygosity was established objectively by typing nine independent DNA microsatellite polymorphisms (polymorphism information content > 0.7), using standard polymerase chain reaction methods and genotyping. Results were cross-checked with blood group (ABO, MNS, and Rh), and phenotypic data (hair, skin, and eye color), giving an overall probability of correct zygosity assignment > 99.99%. Genomic DNA samples were analyzed on the Human610-Quad BeadChip (Illumina) according to the manufacturer's protocols (Infinium HD Assay; Super Protocol Guide; Rev. A, May 2008). For our SNP of interest, rs2710102, 47 (20.1%) were homozygous for the nonrisk allele (TT), 111 (47.4%) subjects were heterozygous for the risk allele (TC), and 76 (32.5%) subjects were homozygous for the risk allele (CC).

Scan acquisition

Whole-brain anatomical and HARDI were collected with a 4T Bruker Medspec MRI scanner. T1-weighted anatomical images were acquired with an inversion recovery rapid gradient echo sequence. The acquisition parameters were as follows: TI/TR/TE = 700/1500/3.35 ms; flip angle = 8°; slice thickness = 0.9 mm, with an acquisition matrix of 256 × 256. Diffusion-weighted images (DWIs) were also acquired using single-shot echo planar imaging with a twice-refocused spin echo sequence to reduce eddy-current induced distortions. The acquisition parameters were optimized to provide the best signal-to-noise ratio (SNR) for estimation of diffusion tensors (Jones et al., 1999). The imaging parameters were as follows: 23 cm FOV, TR/TE 6090/91.7 ms, with a 128 × 128 acquisition matrix. Each three-dimensional (3D) volume consisted of fifty-five 2-mm-thick axial slices with no gap and 1.79 × 1.79 mm^2 in-plane resolution. One hundred five images were acquired per subject: 11 with no diffusion sensitization (i.e., T2-weighted b_0 images) and 94 DWIs (b = 1159 s/mm^2)

with gradient directions evenly distributed on the hemisphere. The scan time for the HARDI scan was 14.2 min.

Cortical extraction and HARDI tractography

Connectivity analysis was performed as in Jahanshad et al. (2011). Briefly, nonbrain regions were automatically removed from each T1-weighted MRI scan, and from a T2-weighted image from the DWI set, using the FSL tool "BET" (FMRIB Software Library, http://fsl.fmrib.ox.ac.uk/fsl/). A trained neuroanatomical expert manually edited the T1-weighted scans to further refine the brain extraction. Total brain volume estimates were obtained from the manually edited full-brain mask, including cerebral, cerebellar, and brainstem regions. All the T1-weighted images were linearly aligned using FSL (with 9 DOF) to a common space (Holmes et al., 1998) with 1 mm isotropic voxels and a 220 × 220 × 220 voxel matrix. Raw DWIs were corrected for eddy current distortions using the FSL tool, "eddy_correct" (http://fsl.fmrib.ox.ac.uk/fsl/). For each subject, the 11 eddy-corrected images with no diffusion sensitization were averaged, linearly aligned, and resampled to a downsampled version of their corresponding T1 image (110 × 110 × 110, 2 × 2 × 2 mm). Averaged b_0 maps were elastically registered to the structural scan using a mutual information cost function (Leow et al., 2005) to compensate for echo planar imaging (EPI)-induced susceptibility artifacts.

Thirty-five cortical labels per hemisphere, as listed in the Desikan–Killiany atlas (Desikan et al., 2006), were automatically extracted from all aligned T1-weighted structural MRI scans using FreeSurfer (http://surfer.nmr.mgh.harvard.edu/). The Desikan–Killiany atlas lists 34 cortical regions per hemisphere that are based on the main cortical gyri, and FreeSurfer adds the insula to make a total of 35 cortical regions for each hemisphere. A complete list of the regions included is found in Jahanshad et al. (2011). Other parcellations are possible, and some may be more sensitive in principle to picking up gene effects. Previous work by our lab found that connectivity maps based on these 70 regions can be used to detect genetic influences on brain connections (in terms of gross heritability rather than SNP effects); so, we planned our SNP analyses based on this parcellation (Jahanshad et al., 2011; Joshi et al., 2010). The Desikan–Killiany atlas has been widely used for structural connectivity analysis (Hagmann et al., 2010; Honey et al., 2009). Even so, there is ongoing work in the field aiming at optimizing the cortical parcellation for network analyses, and at understanding how different parcellation schemes may influence different kinds of network measures (Bassett et al., 2011; Zalesky et al., 2010). Since a linear registration is performed by the software, the resulting T1-weighted images and cortical models were aligned to the original T1 input image space and down-sampled using nearest-neighbor interpolation (to avoid intermixing of labels) to the space of the DWIs. To ensure the tracts intersect cortical labeled boundaries, the labels were dilated with an isotropic box kernel of five voxels.

The transformation matrix from the linear alignment of the mean b_0 image to the T1-weighted volume was applied to each of the 94 gradient directions to properly re-orient the orientation distribution functions (ODFs). At each HARDI voxel, the ODFs were computed using the normalized and dimensionless ODF estimator, derived for q-ball imaging in (Aganj et al., 2010). We performed HARDI tractography on

the linearly aligned sets of DWI volumes using these ODFs. Tractography was performed using the Hough transform method as described in (Aganj et al., 2011). Briefly, tractography was performed after linearly aligning and scaling the DWI data to anatomical (T1-weighted) image space. Since a linear transform was applied to the diffusion-weighted images, we also reoriented the gradient table so that the tract tracing algorithm could correctly follow the dominant direction of diffusion. The table of gradient vectors was corrected to reflect the nonrigid transformation by applying the same transformation to each directional gradient vector. Running tractography after re-orienting the images, as we did here, might slightly affect the SNR of the diffusion signals, as it would act as a very mild spatial filter on the data.

Elastic deformations obtained from the EPI distortion correction, mapping the average b_0 image to the T1-weighted image, were then applied to the tracts' 3D coordinates for accurate alignment of the anatomy. Each subject's dataset contained 2,000–10,000 useable fibers (3D curves). Fibers were filtered to eliminate those likely to be erroneous. All duplicate fibers were removed; those with a very small number of points (<5) were considered unreliable and were also removed.

For each subject, a full 70×70 connectivity matrix was created. Each element described the proportion of the total number of fibers connecting each of the labels; the diagonal elements of the matrix describe the total number of fibers passing through a certain cortical region of interest. Since these values were calculated as a proportion, they were normalized to the total number of fibers traced for each individual participant, so that the results could not be skewed by raw fiber count.

Graph theory analyses

On the 70×70 matrices just generated, we used the Brain Connectivity Toolbox (Rubinov and Sporns, 2010; https://sites.google.com/a/brain-connectivity-toolbox.net/bct/Home) to compute two standard measures of nodal brain connectivity—regional efficiency (EREG) and eccentricity (ECC). EREG is the global efficiency (EGLOB) computed for each node and is related to the clustering coefficient (Latora and Marchiori, 2001). ECC is the longest characteristic path length (CPL) for any given node (Sporns, 2002). We also computed five standard measures of global brain connectivity—CPL, mean clustering coefficient (MCC), EGLOB, small-worldness (SW), and modularity (MOD) (Rubinov and Sporns, 2010). CPL is a measure of the average path length in a network, with path length being the minimum number of edges that should be traversed to get from one node to another. MCC is a measure of how many neighbors of a given node are also connected to each other, in proportion with the maximum number of connections in the network. EGLOB is inversely related to CPL; networks with a small, average CPL are generally more efficient than those with a large, average CPL. SW represents the balance between network differentiation and network integration, calculated as a ratio of local clustering and CPL of a node relative to the same ratio in a randomized network. We created 10 simulated random networks. The ratio of the clustering coefficient in our network to the clustering coefficient in the simulated random networks was denoted by γ (gamma). The ratio of the CPL in

our network to the CPL in the simulated random network was denoted by λ (lambda). These measures were generated in the same way as the others, integrated across a range, and are listed in the results tables alongside MCC and CPL but were not entered into any association analyses. MOD is the degree to which a system can be subdivided into smaller networks (Bullmore and Bassett, 2011). The equations to calculate each of these measures can be found in Rubinov and Sporns (2010).

One step in graph theory analysis is selecting a threshold for the network, termed the sparsity. Networks with a sparsity of 0.2 retain only 20% of the connections of the "full-sparsity" network. Selecting a single sparsity level may arbitrarily affect the network measures, so we computed measures at multiple sparsities, and integrated across that range to generate more stable scores. We calculated these measures for the whole brain over a range of sparsities (0.2–0.3, in 0.01 increments), and calculated the area under the curve of those 11 data points to generate an integrated score for each measure. Twenty-three participants completed two separate scanning sessions 3 months apart in which DTI data were collected. The measures were calculated for both scans for each of these participants over the whole range of sparsities, and we found that the range 0.2–0.3 gave the most stable network measures. Supplementary Figure S1 (Supplementary Data are available online at www.liebertonline.com/brain) shows the calculations of all five network measures plotted for both groups across the sparsity range 0–0.5. These graphs show that at very low sparsities, the graphs are not stable, while we know that higher sparsities are less biologically plausible (Sporns, 2011). We also calculated the network measures for the left and right hemispheres independently. We hypothesized that we would find evidence of altered structural connectivity between the two groups and, thus, started with global graph theory measures of connectivity. We calculated efficiency at a regional level by considering these measures at each node, to see whether our results were attributable to differences in certain brain regions. For these regional measures, we calculated the measures over the same range of sparsities and integrated them over that range. We calculated ECC at a regional level as well. We not only ran *post hoc* association analyses on the raw fiber density matrices to see whether there were overall differences in connectivity but also ran the analyses on a subset of connections, just those with one terminus in the frontal, parietal, or temporal cortex.

Association controlling for relatedness

We performed a mixed-model regression for each network measure to find the association of the SNP while incorporating a model accounting for family relatedness (Kang et al., 2008). When family members are analyzed, the relatedness among members of the sample should be taken into account, and each individual cannot be treated as independent as some share part (in the case of siblings and DZ twins) or all (MZ twins) of their genome. This analysis was performed using Efficient Mixed-Model Association (EMMA; http://mouse.cs.ucla.edu/emma/) within the R statistical package (version 2.9.2; www.r-project.org). A symmetric n×n kinship matrix was constructed to describe the relationship of every subject to all others. A kinship matrix coefficient of 1 denoted

the relationship of each subject to himself/herself; the coefficient for MZ twins within the same family was 1; the coefficient for DZ twins and siblings within the same family was 0.5; and the coefficient for subjects not in the same family was 0. Ancestry outliers were removed, so no additional modeling was used in the kinship matrix to adjust for population genetic structure between families. The association of SNP rs2710102 was tested for all network measures just described according to the following formula:

$$y = X\beta + Zu + e$$

Here, y is a vector representing the network property; X is a matrix of fixed effects containing the genetic effect of the SNP for each subject (coded additively or using other models that combine genotype groups; see above) and a constant term; β is a vector representing the fixed-effect regression coefficients; Z is an identity matrix; u is the random effect with $Var(u) = \sigma_g^2 K$, where K is the kinship matrix; and e is a matrix of residual effects with $Var(e) = \sigma_e^2 I$. Age and sex were included as covariates.

False discovery rate correction for multiple comparisons

All results were controlled for multiple comparisons using the standard false discovery rate (FDR) method (Benjamini and Hochberg, 1995). The FDR is the expected proportion of false positives among results that are declared significant. Simply setting the alpha at a value of 0.05 implies that 5% of the results are expected to be false positives. An FDR q value of 0.05, as used in this article, implies that, on average across experiments, 5% of the results declared significant are expected to be false positives.

Results

Carriers of two (CC) but not just one (CT) risk allele have a higher risk of speech development delay and/or impairment (see SNPedia, at www.snpedia.com/index.php/ Rs2710102). Thus, we coded our analyses in a recessive fashion (with regard to the major risk allele), where individuals homozygous for the risk allele formed one group, and those heterozygous for the risk allele or carrying no copies of the risk allele formed the other group. Graph theory measures depend on a choice of threshold on the strength of connectivity, which may be thought of as a sparsity level: pruning away weaker connections leads to a sparser network model. To avoid this dependency, which could lead to arbitrary thresholding effects in the results, connectivity measures were integrated across a range of sparsities (0.2–0.3), as this range was the most stable in an initial analysis (see Methods section for definitions, and Supplementary Fig. S1). This range of sparsities also makes sense biologically, as demonstrated in a number of studies (Sporns, 2011). All the analyses given next were run on integrated scores calculated in this way.

Results—whole brain measures

We tested associations of the rs2710102 *CNTNAP2* SNP with five commonly studied network measures: CPL, MCC, EGLOB, SW, and MOD. The allele dose at the SNP (i.e., the number of risk alleles) was significantly associated with the CPL in the whole-brain structural network ($b = 0.17$,

$p = 0.0069$), as well as SW ($b = -0.6$, $p = 0.00068$) and EGLOB ($b = -0.09$, $p = 0.00099$) in the left hemisphere and the EGLOB in the right hemisphere ($b = -0.077$, $p = 0.0056$). Here, b represents the unnormalized slope of the regression coefficient, where the at-risk group is coded as 0, and the non-at-risk group is coded as 1. These results remained significant after correcting for multiple comparisons using the FDR procedure (Benjamini and Hochberg, 1995) across all 15 tests performed (5 in the left hemisphere, 5 in the right hemisphere, and 5 for whole brain, $q < 0.05$). Individuals homozygous for the risk allele ($N = 99$) had greater EGLOB in both hemispheres and greater SW in the left hemisphere. Individuals carrying one or no copies of the risk allele ($N = 229$) had a greater CPL in the whole-brain structural network. The whole-brain results, with significant results bolded, along with average values for each group, are shown in Table 1. They are visualized in Figures 1 and 2.

Results—EREG

Our association analysis of the rs2710102 *CNTNAP2* SNP with the EREG of each node, integrated across sparsities .2–.3, yielded results in 11 of the 70 nodes that passed $p < 0.05$ but did not pass the more stringent FDR correction. These results, along with average values for each group, are shown in Table 2. To preserve space, only nodes passing $p < 0.05$ are presented in Table 2.

TABLE 1. GLOBAL RESULTS FROM *CNTNAP2* ASSOCIATION ANALYSIS FOR INTEGRATED GRAPH THEORY METRICS FOR WHOLE BRAIN AND LEFT AND RIGHT HEMISPHERES SEPARATELY

Measure	Risk average (CC)	Nonrisk average (CT and TT)	b	p value
Global measures—recessive model				
Whole brain				
CPL/λ	**17.5**/10.09	**17.67**/10.16	**0.17**	**0.0069**
MCC/γ	8.57/13.74	8.35/14.27	−0.2	0.21
EGLOB	6.16	6.1	−0.049	0.032
SW	13.52	14	0.51	0.021
MOD	5.64	5.53	−0.09	0.12
Left hemisphere				
CPL/λ	19.16/10.67	19.04/10.69	−0.11	0.17
MCC/γ	6.13/17.64	6.16/17.10	0.038	0.54
EGLOB	**5.6**	**5.51**	**−0.09**	**0.00099**
SW	**16.57**	**15.96**	**−0.6**	**0.00068**
MOD	4.54	4.44	−0.098	0.16
Right hemisphere				
CPL/λ	19.02/10.62	18.95/10.66	−0.084	0.3
MCC/γ	6.35/17.37	6.36/17.24	0.02	0.79
EGLOB	**5.64**	**5.56**	**−0.077**	**0.0056**
SW	16.33	16.14	−0.17	0.31
MOD	4.39	4.28	−0.11	0.079

Significant results are bolded. Results pass FDR correction for multiple comparisons across all 15 p values.

Whole-brain results showing *CNTNAP2* SNP associations with graph theory measures of structural connectivity. Results are separated by hemisphere and are shown for the recessive model's SNP effect.

CPL, characteristic path length; MCC, mean clustering coefficient; EGLOB, global efficiency; SW, small-worldness, MOD, modularity; FDR, false discovery rate; SNP, single nucleotide polymorphism.

Results–ECC

To more fully examine the distribution of path lengths in the network, we tested the effect of *CNTNAP2* on ECC, a nodal measure of the maximal shortest path length for each node, meaning the length computed between that node and the farthest node it is connected to. Given the significant results in CPL, EGLOB, and SW, all of which are related to path length, we decided to look further into other measures related to path length. Of course, these are not entirely independent analyses, and should be considered *post hoc* and exploratory. Our analyses of the associations between the rs2710102 *CNTNAP2* SNP and the ECC of each node, integrated across sparsities .2–.3, yielded significant results for 60 of the 70 nodes, 30 in the left hemisphere and 30 in the right hemisphere, as seen in Figure 3 ($q < 0.05$). These results are displayed in Figure 3 along with averages and resultant *b* and *p* values in Table 3. To preserve space, only nodes passing $q < 0.05$ are presented in Table 3.

Post hoc analysis—additive and dominant models

Based on evidence that only carriers of two risk alleles (CC) are affected (see SNPedia, at www.snpedia.com/index.php/Rs2710102), we started with a recessive model, with carriers of the CC genotype forming one group and those with CT or TT forming the other. However, we also ran *post hoc* analyses with the other two possible models: additive, in which each genotype forms one group, and dominant, in which the CC and CT genotypes form one group and participants with the TT genotype form the other group. In the additive model, we detected significant associations between allele dose and CPL in the whole-brain network ($b = 0.10$, $p = 0.0096$), and EGLOB ($b = -0.062$, $p = 0.00041$) and SW ($b = -0.34$, $p = 0.0030$) in the left hemisphere. The global *post hoc* results that survive multiple comparisons correction are presented in Table 4 ($q < 0.05$). For the whole-brain measures in the dominant model, none of the measures were significantly associated with the allele dose at the SNP. For the EREG analyses, the additive model yielded results in 14 nodes ($p < 0.05$), as shown in Supplementary Table S1. The dominant model yielded results in five nodes as well ($p < 0.05$). Neither of these passed FDR correction. These results can be seen in Supplementary Table S2. For the analysis of nodal eccentricities, in the additive model, there were results in 64 of the 70 nodes that passed FDR correction. Six nodes were found to be significant here that had not been originally found in the recessive model, and two were not found in the additive model
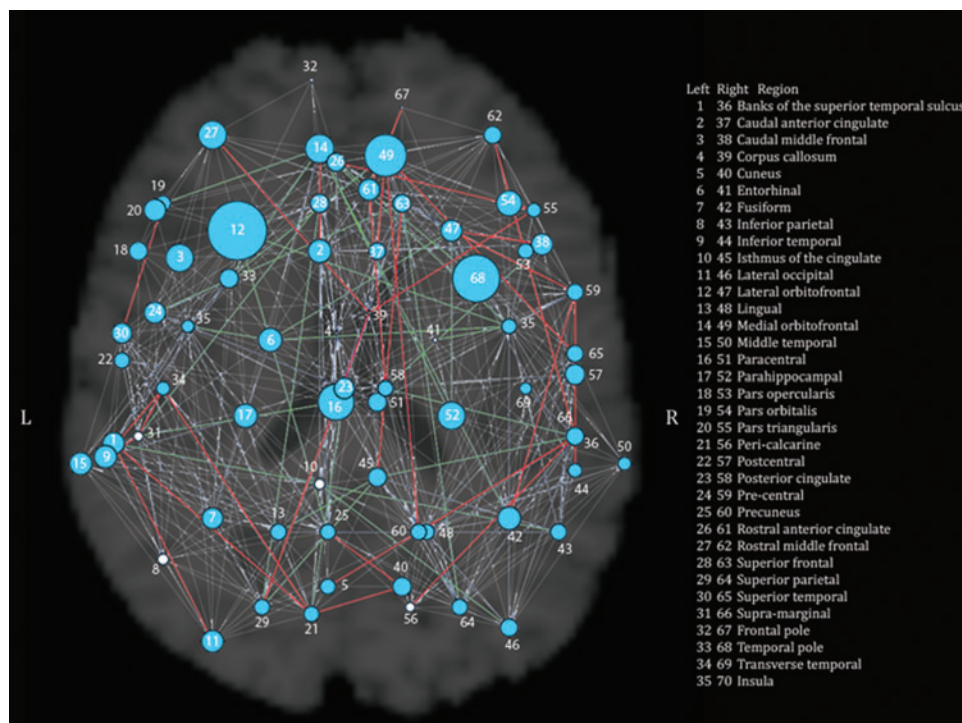

FIG. 1. Global results of *CNTNAP2* association with graph theory metrics for the whole brain. The radius of each node is proportional to the inverse of the *p* value for the comparison between risk (CC) and nonrisk (CT, TT) subjects in the measure of eccentricity. Thus, larger radii indicate nodes showing significant differences between the two groups. Significant nodes are in blue, and nonsignificant nodes are in white. Nodes are labeled with numbers: the legend on the figure lists numbers as they correspond to regions in each hemisphere. Additionally, differences in paths are shown in this figure. Paths that both risk and nonrisk groups have are in gray, those only present in the risk group are in red, and those only present in the nonrisk group are in green. Nodes are labeled with numbers; the legend in the figure lists numbers in each hemisphere as they correspond to regions. Figures 1 and 2 were generated at sparsity = 0.25, using the UCLA Multimodal Connectivity Package (https://github.com/jbrown81/umcp).
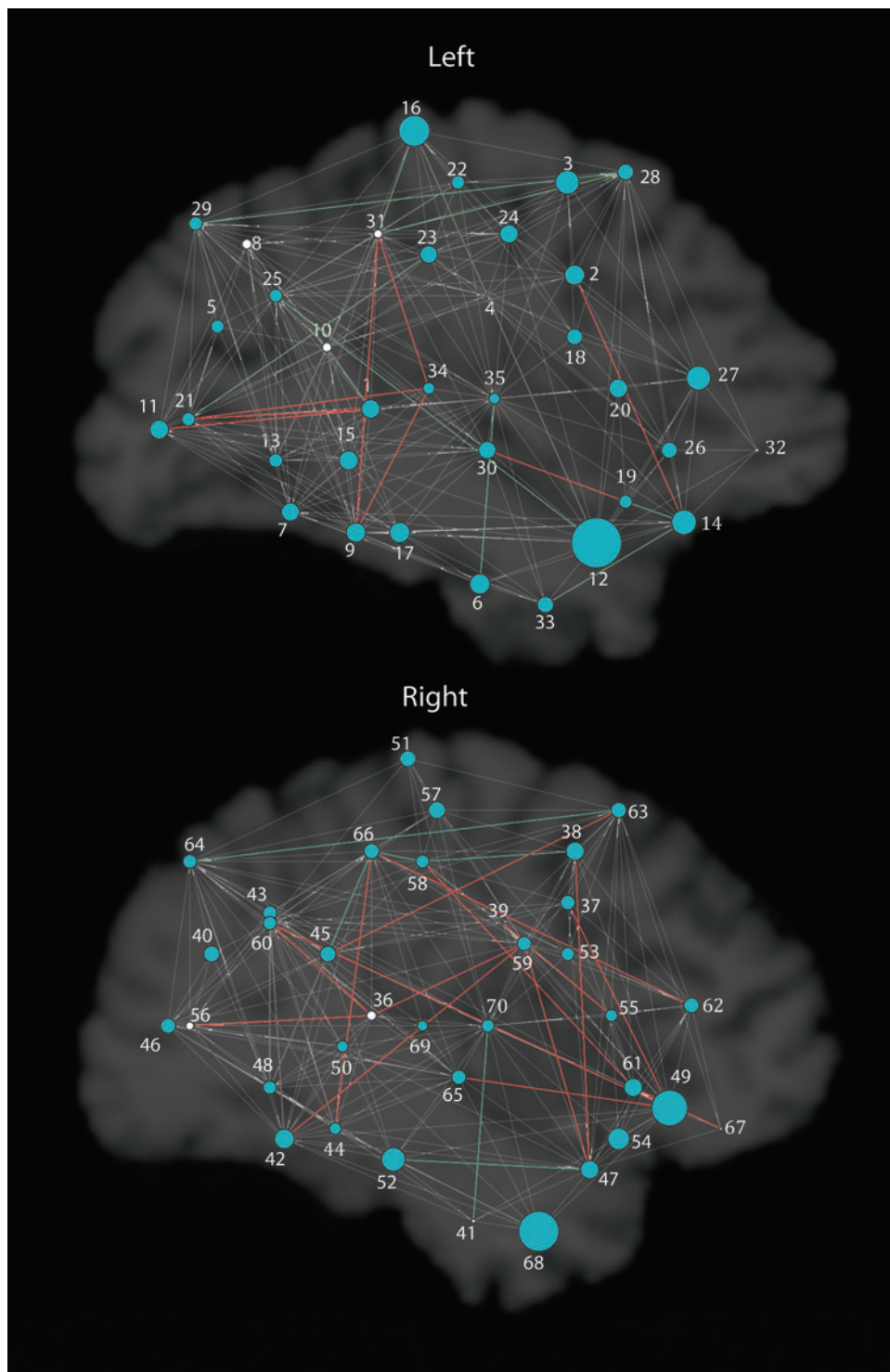
FIG. 2. Global results of *CNTNAP2* association with graph theory metrics for each hemisphere separately. As in Figure 1, larger radii indicate nodes showing significant differences between the two groups in the measure of eccentricity. Significant nodes are in blue, and nonsignificant nodes are in white. Gray paths are present in both groups, red in risk only, and green in nonrisk only. Nodes are labeled with numbers; the legend in the figure lists numbers in each hemisphere as they correspond to regions.

that had been found with the recessive. The two nodes that were significant in the recessive model but not in the additive model were the left fusiform and right insula. The six nodes that were significant in the additive model but not in the recessive model were the left inferior parietal lobule, left isthmus of the cingulate, left supramarginal gyrus, right bank of the superior temporal sulcus, right cuneus, and right pericalcarine cortex. In the dominant model,

there were no significant associations with group membership.

Post hoc analysis—fiber density in frontal, parietal, and temporal lobes and FA

We had initially analyzed whether our two groups differed in their whole fiber density matrices, that is, the number of

TABLE 2. RESULTS FROM INTEGRATED REGIONAL
EFFICIENCY ANALYSIS IN RECESSIVE MODEL

	Regional efficiency–recessive model			
Node	*Risk average (CC)*	*Nonrisk average (CT and TT)*	*b*	*p value*
L caudal anterior cingulate	9.20	8.77	−0.44	0.0061
L caudal middle frontal	8.24	7.78	−0.45	0.0062
L *pars triangularis*	5.63	5.56	−0.060	0.048
L superior frontal	6.63	6.72	0.094	0.0034
L superior parietal	6.32	6.40	0.080	0.0046
L frontal pole	5.36	5.04	−0.27	0.016
R inferior frontal	6.11	6.02	−0.078	0.013
R *pars triangularis*	5.75	5.66	−0.097	0.017
R rostral anterior cingulate	6.00	5.90	−0.11	0.0074
R superior temporal	6.02	5.97	−0.056	0.036
R frontal pole	5.33	4.93	−0.34	0.012

Nonrisk (CT and TT) coded as "1" and risk (CC) coded as "0" such that positive *b* value indicates greater average in nonrisk participants. Only results passing $p < 0.05$ are presented.

Regional efficiency results showing *CNTNAP2* SNP associations with graph theory measures according to recessive model.

L, left; R, right.

fibers per unit volume connecting each node, and found no significant differences. Given the promising findings suggesting associations with global and nodal network measures, we ran *post hoc* tests on the fiber density in the frontal and temporal lobes, where *CNTNAP2* gene expression is enriched (Abrahams et al., 2007; Arking et al., 2008; Strauss et al., 2006; Vernes et al., 2008). In addition, Scott-Van Zeeland et al. had found associations between this gene and measures of functional connectivity in the frontal and parietal lobes; so, we included parietal nodes in this analysis as well. The nodes counted in this subset are listed in Supplementary Table S3. There was a trend for greater fiber density in the nonrisk subjects in all three lobes, but these results did not pass FDR correction. We also checked whether our two groups differed in FA or apparent diffusion coefficient (ADC) along the tracts connecting each node and found no association for any of the connections. One reason we focused our genetic analysis on FA was that we had completed a series of earlier papers that aimed at finding out which DTI-derived measures were most highly heritable. In a twin sample scanned with DTI, it is possible to estimate the proportion of variance in a measure that is attributable to genetic variation, by examining covariances between different types of twins (MZ and DZ). In these early analyses, FA was found to be highly heritable (Lepore et al., 2008) and so were the three diffusion eigenvalues when treated as a multivariate vector (Lee et al., 2009a). The full tensor was also highly heritable, so long as the meaning of heritability was appropriately redefined using a Lie group metric to measure tensor differences (Lee et al., 2009b, 2010). Since FA was more highly heritable than mean diffusivity, we preferred to use it as the target for our subsequent genetic association analyses (Braskie et al., 2011, Jahanshad et al., 2012). In addition, we weighted our fiber density matrices to emphasize those tracts that are expected to be more heavily myelinated by multiplying our fiber density and FA matrices element wise; even so, we
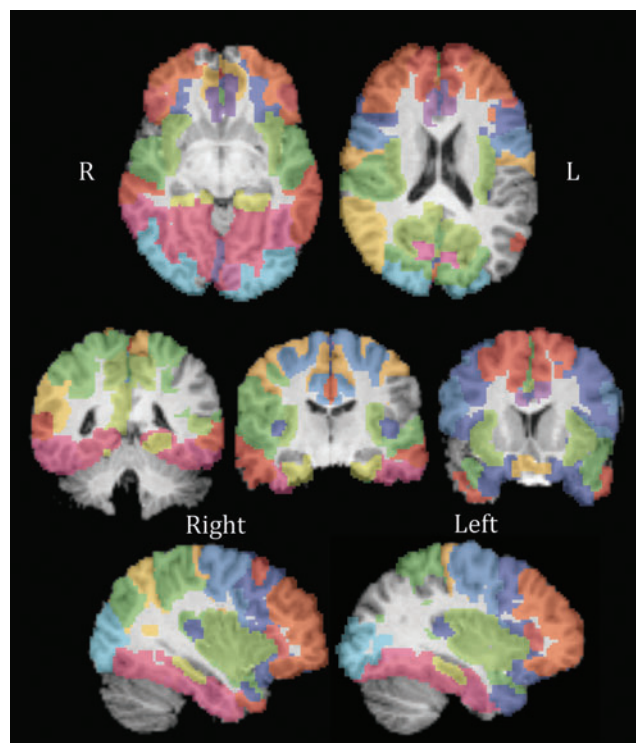

FIG. 3. Image of nodes showing association between eccentricity and the *CNTNAP2* allele dose in the recessive model. Results pass false discovery rate correction for multiple comparisons across all 70 nodes. Colors differentiate each node, with the same color representing one node bilaterally. See Table 3 for color code. From top to bottom, left to right, slices are as follows: Z = 46, Z = 60, Y = 41, Y = 52, Y = 70, X = 36, and X = 72.

found no associations between the *CNTNAP2* dose and those values. Thus, the global and nodal network differences in carriers of the risk gene were not readily reducible to the effects on more common network properties, such as fiber density.

Post hoc analysis—interhemispheric connections

Given evidence that individuals with autism may have abnormalities in interhemispheric connectivity (Just et al., 2007), we generated 35 × 35 matrices of interhemispheric connections for all participants. We analyzed these for differences in fiber density for these interhemispheric connections between the two groups, and found no significant differences that passed FDR correction. We also analyzed whether the number of interhemispheric connections present differed between the groups, meaning the number of elements in the 35 × 35 matrix where >95% of the subjects had nonzero entries, again finding no significant differences.

Discussion

In this study, we found that carriers of a common variant in the autism risk gene, *CNTNAP2,* had differences in structural brain connectivity computed from high-field DTI. Graph theory measures differed in individuals homozygous for the risk allele. This higher-risk group had shorter CPL in the whole-brain network, greater SW and greater EGLOB in the left

TABLE 3. SIGNIFICANT RESULTS FROM INTEGRATED ECCENTRICITY ANALYSIS IN RECESSIVE MODEL

	Eccentricity			
Node	Risk average (CC)	Nonrisk average (CT and TT)	b	p value
L banks of the superior temporal sulcus (lime green)	12.81	15.33	2.4	0.013
L caudal anterior cingulate (purple)	14.21	16.28	2.1	0.011
L caudal middle frontal (dark blue)	16.66	18.79	2.1	0.0078
L cuneus (magenta)	20.96	22.40	1.5	0.026
L entorhinal (green)	21.17	22.38	1.3	0.011
L fusiform (dark magenta)	21.30	22.34	1.0	0.014
L inferior temporal (magenta)	21.66	22.89	1.3	0.012
L lateral occipital (light blue)	21.66	22.95	1.3	0.013
L lateral orbitofrontal (dark blue)	21.16	22.37	1.3	0.0017
L lingual (magenta)	21.63	22.69	1.1	0.023
L medial orbitofrontal (gold)	21.09	22.05	1.0	0.0072
L middle temporal (red)	21.72	23.06	1.3	0.012
L parahippocampal (pale yellow)	21.53	22.79	1.3	0.011
L paracentral (gold)	21.25	22.30	1.1	0.0046
L *pars opercularis* (dark blue)	21.93	23.18	1.3	0.017
L *pars orbitalis* (orange)	22.00	23.41	1.4	0.026
L *pars triangularis* (red)	21.78	23.15	1.4	0.013
L peri-calcarine (pink)	21.67	22.77	1.1	0.025
L postcentral (gold)	21.70	22.83	1.1	0.025
L posterior cingulate (blue)	21.23	22.20	0.93	0.014
L pre-central (blue)	21.41	22.45	1.0	0.013
L precuneus (yellow-green)	21.38	22.28	0.9	0.026
L rostral anterior cingulate (dark purple)	21.36	22.38	1.0	0.018
L rostral middle frontal (orange)	21.50	22.73	1.2	0.0075
L superior frontal (red)	21.29	22.23	0.93	0.017
L superior parietal (green)	21.50	22.48	1.0	0.024
L superior temporal (forest green)	21.71	22.91	1.2	0.015
L temporal pole (dark blue)	21.85	23.17	1.3	0.017
L transverse temporal (dark blue)	21.98	23.53	1.4	0.032
L insula (lime green)	21.53	22.45	0.9	0.038
R caudal anterior cingulate (purple)	21.46	22.58	1.0	0.021
R caudal middle frontal (dark blue)	21.37	22.42	1.0	0.013
R cuneus (magenta)	21.77	23.10	1.3	0.017
R fusiform (dark magenta)	21.19	22.22	1.0	0.011
R inferior parietal (yellow)	21.44	22.46	1.0	0.023
R inferior temporal (magenta)	21.55	22.72	1.1	0.031
R isthmus of the cingulate (lime green)	21.28	22.39	1.0	0.017
R lateral occipital (light blue)	21.45	22.47	1.0	0.02
R lateral orbitofrontal (dark blue)	21.17	22.25	1.0	0.013
R lingual (magenta)	21.42	22.47	1.0	0.025
R medial orbitofrontal (gold)	21.02	22.03	1.1	0.0034
R middle temporal (red)	21.80	23.01	1.2	0.034
R parahippocampal (pale yellow)	21.41	22.70	1.3	0.0078
R paracentral (gold)	21.35	22.36	1.0	0.017
R *pars opercularis* (dark blue)	21.83	23.21	1.3	0.025
R *pars orbitalis* (orange)	21.80	23.44	1.8	0.0093
R *pars triangularis* (red)	21.83	23.09	1.3	0.03
R postcentral (gold)	21.46	22.59	1.1	0.015
R posterior cingulate (blue)	21.36	22.26	0.87	0.026
R pre-central (blue)	21.34	22.29	0.92	0.022
R precuneus (yellow-green)	21.33	22.29	0.91	0.024
R rostral anterior cingulate (dark purple)	21.41	22.54	1.1	0.013
R rostral middle frontal (orange)	21.46	22.55	1.1	0.019
R superior frontal (red)	21.29	22.25	0.93	0.019
R superior parietal (green)	21.39	22.35	0.92	0.024
R superior temporal (forest green)	21.79	23.04	1.3	0.021
R supra-marginal (green)	21.61	22.74	1.1	0.019
R temporal pole (dark blue)	21.45	23.19	1.8	0.0027
R transverse temporal (dark blue)	22.24	23.57	1.3	0.042
R insula (lime green)	21.45	22.40	0.93	0.027

Nonrisk coded as "1" and risk coded as "0"; *b* value represents gain in eccentricity for nonrisk group (CT and TT) compared with risk group (CC). All passing FDR corrected across all 70 nodes tested (*q* < 0.05). Only significant results are presented. Colors refer to Figure 3.

Regional results showing *CNTNAP2* SNP associations with node eccentricity.

L, left; R, right.

Table 4. Results from *Post hoc* Analyses of Additive Models for Integrated Global Measures That Pass False Discovery Rate

Global measures–additive model					
Measure	CC	CT	TT	b	p value
Whole Brain					
CPL	17.47	17.68	17.7	0.10	0.0096
Left Hemisphere					
EGLOB	5.56	5.52	5.53	−0.062	0.00041
SW	16.32	16.04	16.14	−0.34	0.003

Post hoc analyses of the additive model passing FDR.

hemisphere, and greater EGLOB in the right hemisphere. These results may seem counter-intuitive given findings of higher efficiency, but higher efficiency in structural networks may reflect more random connections in the risk-group's brain networks, as random networks have high levels of EGLOB (Bullmore and Sporns, 2009). Further analysis at the nodal level revealed that the homozygous at-risk participants had lower ECC across 60 of the 70 network nodes in the non-risk participants, and borderline significant results (passed $p < 0.05$ but not FDR correction) in EREG in 11 of the 70 nodes. A final analysis attempted to further simplify the results by assessing FA and fiber density differences, but did not detect associations with these more common fiber measures. In other words, several global and nodal properties of the structural network were different in carriers of the risk gene, but they were not attributable to more common characteristics of fibers, such as fiber density or FA. A larger sample size might detect differences in FA in carriers of the risk gene, but our findings suggest that differences are more prominent at the network level.

In their recent study, Scott-Van Zeeland et al. (2010) found that a *CNTNAP2* SNP was associated with differences in the functional connectivity of frontal and parietal cortical networks, including effects on the strength of short- and long-range connections to the frontal and parietal cortex. In this case, the range reflected the physical distance between two regions, while in graph theory, distance instead reflects the number of paths between one node and another. While path distance and physical distance are not the same, they both indicate distance between one brain region and another. Since this is the property measured by CPL and EGLOB using graph theoretical methods, we hypothesized that we could assess corresponding measures from structural networks using DTI, and that these measures might be altered in carriers of the *CNTNAP2* risk allele. We found that carriers have altered structural connectivity—as measured by a number of graph theory metrics—which may partly underlie the alterations in functional connectivity.

SW is a well-developed concept from graph theory (Watts and Strogatz, 1998) that has more recently been applied to brain networks (Sporns et al., 2004). A network with high SW has high local clustering and a short CPL. Subjects homozygous for the risk allele had greater SW and greater EGLOB in their left hemispheres, which are both driven in part or wholly by shorter CPLs. Risk subjects also had higher EGLOB in the right hemisphere as well as shorter CPL at a whole-brain level. Since there were no significant differences in clustering,

differences in path length may drive the observed differences in SW. Greater efficiency in those at risk is unexpected, as Hagmann et al. (2010) found greater efficiency as development progressed, and Pollonini et al. (2010) found decreased EGLOB in autistic subjects. However, Hagmann et al. based their calculations on 1/ADC, while we based ours on fiber density, and Pollonini et al. was a magnetoencephalography (MEG) study with Granger causality, so the comparison is not direct. A random network has high efficiency (Bullmore and Sporns, 2009), but it may not be functionally advantageous if the proper connections are not made. Neural network complexity is typically achieved by a balance of randomness and regularity—at either extreme, you have a system less able to learn, because it is either never stable enough to remember or never flexible enough to adapt (Sporns, 2011). A more random network, while having a shorter average path length, will be less complex, and arguably further from ideal in terms of brain function. A more random network, while having a shorter average path length, will be less complex, and may not reflect the organization found in real functional brain networks. Individuals differ widely in brain structure and function, but complete "randomness" of connections is not typical of functional circuitry in the brain. A random network, with no stability in time or logical set up, does not tend to make the most efficient use of the brain's resources (Chialvo, 2010). While additional studies are required, higher EGLOB may reflect more random connections in the structural networks of the at-risk participants, as random networks have low path lengths.

Based on our global results, we decided to look further into various nodal measures of connectivity. In these *post hoc* tests, we found a significant association between *CNTNAP2* allele dose and the ECC at 60 of the 70 nodes, with nonrisk carriers having greater ECC across all nodes. ECC is the distance, in paths traversed, between a given node and the node farthest from it (Sporns, 2002). Nonrisk participants had greater ECC across most of the brain. Studies of ECC in brain networks are few (Pollonini et al., 2010) and have not generated any significant results so far; so, we have little context for these results. However, given that they are across a majority of nodes in the brain, they could underlie the global trends we found as well. We found 11 nodes with borderline significant differences (passed $p < 0.05$ but not FDR correction) in EREG, 8 of which were in the frontal lobe, 2 in the temporal lobe, and 1 in the parietal lobe. These are the areas where *CNTNAP2* expression is especially enriched (Abrahams et al., 2007; Arking et al., 2008; Strauss et al., 2006; Vernes et al., 2008) and where Scott-Van Zeeland found differences in functional connectivity.

In attempting to discover a simpler underlying cause of these results, we looked into possible differences in the fiber density matrices of the two groups. We had initially ruled out differences in overall connectivity by running our analysis of *CNTNAP2* on the whole fiber density matrices. However, in trying to understand our results of greater EGLOB and shorter CPL in the risk allele carriers, we decided to look only at those connections with at least one terminus in the frontal, parietal, or temporal lobes. While we found a trend for greater fiber density in the nonrisk subjects in a large number of frontal, parietal, and temporal connections, these results did not pass FDR correction. Tan et al. (2010) conducted a study of a different *CNTNAP2* SNP, rs7794745, in a large cohort of healthy subjects as well. Regional gray and white matter volumes were lower in those homozygous for the risk allele. We will continue

to search for an explanation for our unexpected findings, but currently they do not appear to be reducible to more simple measures of structural connectivity.

Our findings relating a common risk variant in *CNTNAP2* with structural connectivity suggests that the protein it codes for, CASPR2, may be involved in white matter tract structure. This seems likely, as CASPR2 has a role in neuroblast migration (Strauss et al., 2006) and in stabilizing K^+ channels in the juxtaparanodal region (Poliak et al., 1999, 2003). *CNTNAP2* risk allele carriers may have aberrant neuroblast migration or K^+ channel clustering early in development; this may even underlie the differences we see in structural connectivity. Abnormal neuronal migration early in development could lead to altered development of white matter, leading to the changes we see. Abnormal K^+ channel clustering could affect axonal physiology for developing tracts, perhaps even affecting overall tract structure. The recent study characterizing the *CNTNAP2* knockout found, along with various behavioral hallmarks of autism, neuronal migration abnormalities, including abnormal clustering of neurons in the deep layers of the cortex (Peñagarikano et al., 2011). *CNTNAP2* is a risk gene for autism, but it also has effects in nonautistic populations with language disorders. It may be more appropriate to consider it as a risk gene for language difficulties—a key component of autism. A disorder as complex and varied as autism most likely results from a constellation of genetic variations interacting with environmental influences (Szatmari et al., 2007). The SNP rs2710102 in *CNTNAP2* may be one of these polymorphisms that, when combined with others, could increase te risk for autism by increasing the susceptibility to language difficulties. In this article, our focus was the effects of *CNTNAP2* on brain structural connectivity. Understanding why a gene increases risk for a disorder is as crucial as determining that it increases risk in the first place, as a more mechanistic understanding is necessary for ultimately developing interventions. Here, we discovered a mechanistic clue that might explain the association between *CNTNAP2* and autism and language disorders. This altered connectivity may represent an intermediate phenotype for one source of language difficulties. Our participants were a large cohort of twins screened for psychiatric disorders and developmental conditions; thus, they fall within the normal range of language ability.

Of the three different models, the recessive model yielded the strongest results. We chose this model based on information that individuals with the CC genotype have an increased risk of language impairment (www.snpedia.com/index.php/Rs2710102). However, Scott-Van Zeeland's study supports a dominant effect of the *CNTNAP2* SNP. Vernes et al. (2008) found that a haplotype of nine SNPs, including this *CNTNAP2* SNP, had a dominant effect, but no other studies have produced evidence on the dominance of *CNTNAP2* rs2710102 by itself. Our analyses were based on healthy subjects, while previous studies have been conducted on autistic or language-impaired participants, so we followed our analyses with *post hoc* tests to check the other two models in case the effect differed from that in our healthy population.

Conclusions

In this study, the first to link graph theory measures of brain structural connectivity with a specific genetic variant associated with autism, we searched for structural differences that might contribute to the reported effects of *CNTNAP2* on functional networks. In our large cohort of healthy adults, the same *CNTNAP2* SNP was also associated with detectable differences in structural connectivity. In comparing findings from different imaging modalities, these efforts lead to a better understanding of genetic liability for autism and related disorders. Our results not only add to previous work on the effects of *CNTNAP2* on brain structure but also raise new questions regarding the underlying difference. A new approach to neuroimaging genetics is combining multiple polymorphisms–in the same or different genes—when testing for associations with phenotypes, leading to increased predictive accuracy (Chiang et al., 2011b; Hibar et al., 2011). Studies using this method have already been conducted on another autism risk gene (Kohannim et al., in review) that was a top hit in a genome-wide scan for risk alleles (Anney et al., 2010). *CNTNAP2* is classified as an autism risk gene, but we have shown that it has effects in a healthy population as well. These results will further our understanding of how vulnerabilities for various genetically influenced disorders are displayed in the brain.

Author Contributions

K.L.M., G.I.d.Z., G.M., N.G.M., and M.J.W. collected the data. E.L.D., N.J., J.D.R., J.A.B., and P.M.T. analyzed the data. E.L.D., N.J., and P.M.T. wrote the initial manuscript draft. All authors contributed to revisions and commented on drafts.

Author Disclosure Statement

The authors have no competing financial interests.

References

Abrahams BS, Tentler D, Perederiy JV, Oldham MC, Coppola G, Geschwind DH. 2007. Genome-wide analyses of human perisylvian cerebral cortical patterning. Proc Natl Acad Sci U S A 104:17849–17854.

Aganj I, Lenglet C, Jahanshad N, Yacoub E, Harel N, Thompson PM, Sapiro G. 2011. A Hough transform global probabilistic approach to multiple-subject diffusion MRI tractography. Med Image Analysis 15:414–425.

Aganj I, Lenglet C, Sapiro G, Yacoub E, Ugurbil K, Harel N. 2010. Reconstruction of the orientation distribution function in single- and multiple-shell q-ball imaging within constant solid angle. Magn Reson Med 64:554–566.

Alarcón M, Abrahams BS, Stone JL, Duvall JA, Perederiy JV, Bomar JM, Sebat J, Wigler M, Martin CL, Ledbetter DH, Nelson SF, Cantor RM, Geschwind DH. 2008. Linkage, association, and gene-expression analyses identify CNTNAP2 as an autism-susceptibility gene. Am J Hum Genet 82:150–159.

Annett M. 1970. A classification of hand preference by association analysis. Br J Psychol 61:303–321.

Anney R, Klei L, Pinto D, et al. 2010. A genome-wide scan for common alleles affecting risk for autism. Hum Mol Genet 19:4072–4082.

Arking D, Cutler D, Brune CW, Teslovich TM, West K, Ikeda M, Rea A, Guy M, Lin S, Cook Jr., EH, Chakravarti A. 2008. A common genetic variant in the neurexin superfamily member CNTNAP2 increases familial risk of autism. Am J Hum Genet 82:160–164.

Bakkaloglu B, O'Roak B, Louvi A, Gupta AR, Abelson JF, Morgan TM, Chawarska K, Klin A, Ercan-Sencicek AG, Stillman AA, Tanriover G, Abrahams BS, Duvall JA, Robbins EM, Geschwind DH, Biederer T, Gunel M, Lifton RP, State MW. 2008. Molecular cytogenetic analysis and resequencing of contactin associated protein-like 2 in autism spectrum disorders. Am J Hum Genet 82:165–173.

Bassett DS, Brown JA, Deshpande V, Carlson JM, Grafton ST. 2011. Conserved and variable architecture of human white matter connectivity. NeuroImage 54:1262–1279.

Baynes K, Eliassen J, Lutsep HL, Gazzaniga MS. 1998. Modular organization of cognitive systems masked by interhemispheric integration. Science 280:902–905.

Benjamini Y, Hochberg Y. 1995. Controlling the false discovery rate: a practical and powerful approach to multiple testing. J R Stat Soc B 57:289–300.

Braskie M, Jahanshad N, Stein J, Barysheva M, McMahon K, de Zubicaray GI, Martin NG, Wright MJ, Ringman JM, Toga AW, Thompson PM. 2011. Common Alzheimer's disease risk variant within the CLU gene affects white matter microstructure in young adults. J Neurosci 31:6764–6770.

Bullmore E, Bassett D. 2011. Brain graphs: graphical models of the human brain connectome. Annu Rev Clin Psychol 7:113–140.

Bullmore E, Sporns O. 2009. Complex brain networks: graph theoretical analysis of structural and functional systems. Nat Rev Neurosci 10:186–198.

Chialvo DR. 2010. Emergent complex neural dynamics. Nat Phys 6:744–750.

Chiang M-C, Avedissian C, Barysheva M, Toga A, McMahon K, de Zubicaray GI, Wright MJ, Thompson PM. 2009. Extending genetic linkage analysis to diffusion tensor images to map single gene effects on brain fiber architecture. Med Image Comput Comput Assist Interv MICCAI 12:506–513.

Chiang M-C, McMahon KL, de Zubicaray GI, Martin NG, Hickie I, Toga A, Wright MJ, Thompson PM. 2011a. Genetics of white matter development: a DTI study of 705 twins and their siblings aged 12 to 29. NeuroImage 54:2308–2317.

Chiang MC, McMahon KL, de Zubicaray GI, Martin NG, Toga AW, Wright MJ, Thompson PM. Hierarchical Clustering of the Genetic Connectivity Matrix Reveals the Network Topology of Gene Action on Brain Microstructure. In Proceedings of the 8th IEEE ISBI, Chicago, Illinois, USA, 2011b, pp. 832–835.

de Zubicaray GI, Chiang M-C, McMahon KL, Shattuck DV, Toga AW, Martin NG, Wright MJ, Thompson PM. 2008. Meeting the challenges of neuroimaging genetics. Brain Imaging Behav 2:258–263.

Dennis EL, Jahanshad N, Toga A, Brown J, Rudie J, Bookheimer S, Dapretto M, Johnson K, McMahon K, de Zubicaray G, Martin N, Wright M, Thompson P. Heritability of Structural Brain Connectivity Network Measures in 188 Twins. In Proceedings of the 41st Annual Meeting of the Society for Neuroscience, Washington, D.C., USA, 12 to 16 November 2011.

Desikan RS, Ségonne F, Fischl B, Quinn BT, Dickerson BC, Blacker D, et al. 2006. An automated labeling system for sub-dividing the human cerebral cortex on MRI scans into gyral based regions of interest. NeuroImage 31:968–980.

Dosenbach NUF, Nardos B, Cohen AL, Fair DA, Power JD, Church JA, Nelson SM, Wig GS, Vogel AC, Lessov-Schlaggar CN, Barnes KA, Dubis JW, Feczko E, Coalson RS, Pruett JR, Barch DM, Petersen SE, Schlaggar BL. 2010. Prediction of individual brain maturity using fMRI. Science 329:1358–1361.

Hagmann P, Sporns O, Madan N, Cammoun L, Pienaar R, Wedeen VJ, Meuli R, Thiran JP, Grant PE. 2010. White matter maturation reshapes structural connectivity in the late developing human brain. Proc Natl Acad Sci U S A 107:19067–19072.

Hibar D, Kohannim O, Stein JL, Chiang MC, Thompson PM. 2011. Multilocus Genetic Analysis of Brain Images. Front Genet 2:73 .

Holmes CJ, Hoge R, Collins L, Woods R, Toga AW, Evans AC. 1998. Enhancement of MR images using registration for signal averaging. J Comput Assist Tomogr 22:324–333.

Honey CJ, Sporns O, Cammoun L, Gigandet X, Thiran JP, Meuli R, Hagmann P. 2009. Predicting human resting-state functional connectivity from structural connectivity. Proc Natl Acad Sci U S A 106:2035–2040.

Huttenlocher PR. 1990. Morphometric study of human cerebral cortex development. Neuropsychologia 28:517–527.

Jahanshad N, Aganj I, Lenglet C, Jin Y, Joshi A, Barysheva M, McMahon KL, de Zubicaray GI, Martin NG, Wright MJ, Toga AW, Sapiro G, Thompson PM, High Angular Resolution Diffusion Imaging (HARDI) Tractography in 234 Young Adults Reveals Greater Frontal Lobe Connectivity in Women. In Proceedings of the 8th IEEE ISBI, Chicago, Illinois, USA, 2011, pp. 939–943.

Jahanshad N, Kohannim O, Hiber DP, Stein JL, McMahon KL, de Zubicaray GI, Medland SE, Montgomery GW, Whitfield JB, Martin NG, Wright MJ, Toga AW, Thompson PM. 2012. Brain structure in healthy adults is related to serum transferrin and the H63D polymorphism in the *HFE* gene. Proc Natl Acad Sci U S A [Epub ahead of print].

Jahanshad N, Lee A, Barysheva M, McMahon KL, de Zubicaray GI, Martin NG, Wright MJ, Toga AW, Thompson PM. 2010. Genetic influences on brain asymmetry: a DTI study of 374 twins and siblings. NeuroImage 52:455–469.

Jones DK, Horsfield MA, Simmons A. 1999. Optimal strategies for measuring diffusion in anisotropic systems by magnetic resonance imaging. Magn Reson Med 42:515–525.

Joshi AA, Lepore N, Joshi S, Lee AD, Barysheva M, de Zubicaray GI, Wright MJ, McMahon KL, Toga AW, Thompson PM. A Genetic Analysis of Cortical Thickness in 372 Twins. In Proceedings of the 7th IEEE ISBI, Rotterdam, The Netherlands, 2010, pp. 101–104.

Just MA, Cherkassky VL, Keller TA, Kana RK, Minshew NJ. 2007. Functional and anatomical cortical underconnectivity in autism: evidence from an fMRI study of an executive function task and corpus callosum morphometry. Cereb Cortex 17:951–961.

Kang HM, Zaitlen NA, Wade CM, Kirby A, Heckerman D, Daly MJ, Eskin E. 2008. Efficient control of population structure in model organism association mapping. Genetics 178:1709–1723.

Kohannim O, Jahanshad N, Braskie MN, Stein JL, Chiang M-C, Reese AH, Hibar DP, Toga AW, McMahon KL, de Zubicaray GI, Medland SE, Wright MJ, Thompson PM. 2011. Predicting white matter integrity from multiple common genetic variants. Neuropsycopharmacology (accepted).

Latora V, Marchiori M. 2001. Efficient behavior of small-world networks. Phys Rev Lett 87:198701.

Lee AD, Lepore N, Brun CC, Barysheva M, Chou YY, Chiang MC, Madsen SK, McMahon KL, de Zubicaray GI, Wright MJ,

Toga AW, Thompson PM. The Multivariate A/C/E Model and the Genetics of Fiber Architecture. In Proceedings of the 6th IEEE ISBI, Boston, Massachusetts, 2009a, pp. 125–128.

Lee AD, Lepore N, Brun CC, Chou YY, Barysheva M, Chiang MC, Madsen SK, de Zubicaray GI, McMahon KL, Wright MJ, Toga AW, Thompson PM. Tensor-Based Analysis of Genetic Influences on Brain Integrity using DTI in 100 Twins, Medical Image Computing and Computer Assisted Intervention. In Proceedings of the 12th MICCAI, London, United Kingdom, 2009b, pp. 967–974.

Lee AD, Lepore N, de Leeuw J, Brun CC, Barysheva M, McMahon KL, de Zubicaray GI, Martin NG, Wright MJ, Thompson PM. Multivariate Variance-Components Analysis in DTI. In Proceedings of the 7th IEEE ISBI, Rotterdam, The Netherlands, 2010, pp. 1157–1160.

Leow A, Huang S-C, Geng A, Becker J, Davis S, Toga A, Thompson P. 2005. Inverse consistent mapping in 3D deformable image registration: its construction and statistical properties. Inf Process Med Imaging 19:493–503.

Lepore N, Brun CC, Chou YY, Lee AD, Barysheva M, de Zubicaray GI, Meredith M, McMahon K, Wright MJ, Toga AW, Thompson PM. Multi-Atlas Tensor-Based Morphometry and its Application to a Genetic Study of 92 Twins. Workshop on Mathematical Foundations of Computational Anatomy, International Conference on Medical Image Computing and Computer Assisted Intervention (MICCAI), New York, New York, September 6 (2008).

McIntosh AM, Moorhead TWJ, Job D, Lymer GKS, Muñoz Maniega S, McKirdy J, Sussman JED, Baig BJ, Bastin ME, Porteous D, Evans KL, Johnstone EC, Lawrie SM, Hall J. 2008. The effects of a neuregulin 1 variant on white matter density and integrity. Mol. Psychiatry 13:1054–1059.

Peñagarikano O, Abrahams BS, Herman EI, Winden KD, Gdalyahu A, Dong H, Sonnenblick LI, Gruver R, Almajano J, Bragin A, Golshani P, Trachtenberg JT, Peles E, Geschwind DH. 2011. Absence of CNTNAP2 leads to epilepsy, neuronal migration abnormalities, and core autism-related deficits. Cell 147:235–246.

Pfefferbaum A, Sullivan EV, Carmelli D. 2001. Genetic regulation of regional microstructure of the corpus callosum in late life. NeuroReport 12:1677–1681.

Poliak S, Gollan L, Martinez R, Custer A, Einheber S, Salzer JL, Trimmer JS, Shrager P, Peles E. 1999. Caspr2, a new member of the Neurexin superfamily, is localized at the juxtaparanodes of myelinated axons and associated with K+ channels. Neuron 24:1037–1047.

Poliak S, Salomon D, Elhanany H, Sabanay H, Kiernan B, Pevny L, Stewart CL, Xu X, Chiu S-Y, Shrager P, Furley AJW, Peles E. 2003. Juxtaparanodal clustering of Shaker-like K+ channels in myelinated axons depends on Caspr2 and TAG-1. J Cell Biology 162:1149–1160.

Pollonini L, Patidar U, Situ N, Rezaie R, Papanicolaou AC, Zouridakis G. Functional Connectivity Networks in the Autistic and Healthy Brain Assessed Using Granger Causality. In Proceedings of the 32nd IEEE EMBS, Buenos Aires, Argentina, 2010, pp. 1730–1733.

Posthuma D, De Geus EJC, Neale MC, Hulshoff Pol HE, Baaré WEC, Kahn RS, Boomsma D. 2000. Multivariate genetic analysis of brain structure in an extended twin design. Behav Genet 30:311–319.

Rubinov M, Sporns O. 2010. Complex network measures of brain connectivity: uses and interpretations. NeuroImage 52:1059–1069.

Schmitt JE, Lenroot RK, Wallace GL, Ordaz S, Taylor KN, Kabani N, Greenstein D, Lerch JP, Kendler KS, Neale MC, Giedd JN. 2008. Identification of genetically mediated cortical networks: a multivariate study of pediatric twins and siblings. Cereb Cortex 18:1737–1747.

Scott-Van Zeeland A, Abrahams B, Alvarez-Retuerto A, Sonnenblick L, Rudie J, Ghahremani D, Mumford JA, Poldrack RA, Dapretto M, Geschwind DH, Bookheimer SY. 2010. Altered functional connectivity in frontal lobe circuits is associated with variation in the autism risk gene CNTNAP2. Sci Transl Med 2:1–6.

Sporns O. 2002. Graph theory methods for the analysis of neural connectivity patterns, In: Kötter R (ed.) *Neuroscience Databases. A Practical Guide*. Boston, MA: Klüwer; pp. 171–186.

Sporns O. 2011. *Networks of the Brain*. Cambridge, MA: The MIT Press.

Sporns O, Chialvo DR, Kaiser M, Hilgetag CC. 2004. Organization, development and function of complex brain networks. Trends Cogn Sci 8:418–425.

Stein JL, Medland SE, Vasquez AA, et al. 2012. Common genetic polymorphisms contribute to the variation in human hippocampal and intracranial volume. Nat Genet (in press).

Stein MB, Yang B-Z, Chavira DA, Hitchcock CA, Sung SC, Shipon-Blum E, Gelernter J. 2011. A common genetic variant in the Neurexin superfamily member CNTNAP2 is associated with increased risk for selective mutism and social anxiety-related traits. Biol Psychiatry 69:825–831.

Strauss K, Puffenberger E, Huentelman M, Gottlieb S, Dobrin S, Parod J, et al. 2006. Recessive symptomatic focal epilepsy and mutant contactin-associated protein-like 2. N Engl J Med 354:1370–1377.

Szatmari P, Paterson A, Zwaigenbaum L, et al. 2007. Mapping autism risk loci using genetic linkage and chromosomal rearrangements. Nat Genet 39:319–328.

Tan G, Doke T, Ashburner J, Wood N, Frackowiak R. 2010. Normal variation in fronto-occipital circuitry and cerebellar structure with an autism-associated polymorphism of CNTNAP2. NeuroImage 53:1030–1042.

Thompson PM, Cannon TD, Narr KL, van Erp T, Poutanen VP, Huttunen M, Lonnqvist J, Standertskjold-Nordenstam CG, Kaprio J, Khaledy M, Dail R, Zoumalan CI, Toga AW. 2001. Genetic influences on brain structure. Nat Neurosci 4:1253–1258.

Vernes SC, Newbury DF, Abrahams BS, Winchester L, Nicod J, Gorszner M, Alarcón M, Oliver PL, Davies KE, Geschwind DH, Monaco AP, Fisher SE. 2008. A functional genetic link between distinct developmental language disorders. N Engl J Med 359:2337–2345.

Watts DJ, Strogatz SH. 1998. Collective dynamics of "small-world" networks. Nature 393:440–442.

Winterer G, Konrad A, Vucurevic G, Musso F, Stoeter P, Dahmen N. 2008. Association of the 5' end neuregulin-1 (NRG1) gene variation with subcortical medial frontal microstructure in humans. NeuroImage 40:712–718.

Zalesky A, Fornito A, Harding IH, Cocchi L, Yücel M, Pantelis C, Bullmore ET. 2010. Whole-brain anatomical networks: does the choice of nodes matter? NeuroImage 50:970–983.

Address correspondence to:
Paul M. Thompson
Department of Neurology
Laboratory of Neuro Imaging
UCLA School of Medicine
635 Charles Young Drive South
Suite 225
Los Angeles, CA 90095-7334

E-mail: thompson@loni.ucla.edu